Effect of geodetic precession on pulsar high-energy emission

Confronting slot gaps, outer gaps and striped wind

Jérôme Pétri[1]

[1]Observatoire astronomique de Strasbourg, Université de Strasbourg, France.

PROJET FINANCÉ PAR L'ANR - PROJECT FUNDED BY THE ANR

Summary

1. Context & Objectives
2. Model
   - geodetic precession
   - striped wind
3. Application to high-energy pulsed emission
   - theoretical expectations
   - pulsar best candidates
4. Conclusion & Perspectives

Context & Goal

Context

- geodetic precession directly observed in the double-pulsar PSR J0737-3039.
- rate measured and agrees with predictions of general relativity.
- very recently, double pulsar detected in X-rays and gamma-rays.
- fuels the hope observing geodetic precession in high-energy.
- but, geometric configuration renders detection of such effect unlikely.
- however, geodetic precession present in other relativistic binaries or double neutron star systems containing at least one X-ray or gamma-ray pulsar.

Goal

- compute variation of high-energy pulse profile expected from geodetic motion.
- compare striped wind to two-pole caustic and outer gap emission patterns.

Geodetic precession

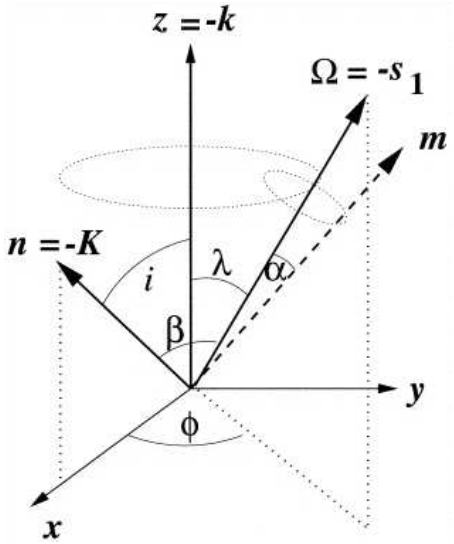

Figure: Geometry of geodetic precession (Kramer, 1998).

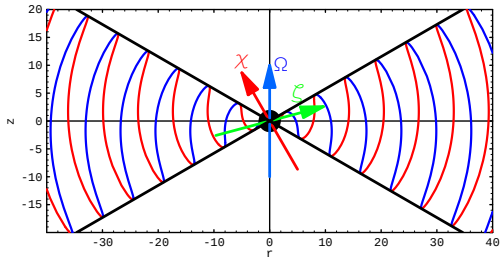

Figure: Viewing geometry (Petri, 2012).

Evolution of the inclination of the line of sight ζ with respect to precession phase

(Damour & Taylor, 1992; Kramer, 1998)

$$\cos\zeta = \cos\delta\,\cos i + \sin\delta\,\sin i\,\cos\Omega_{\rm p}\,(t - t_0).$$

- ζ inclination of the line of sight.
- i angle between orbital plane and line of sight.
- δ angle formed by orbital momentum **L** and rotation Ω.
- $\Omega_{\rm p}$ precession frequency.
- t time with respect to some reference t_0.

$$\Omega_{\rm p} = \left(\frac{2\,\pi}{P_b}\right)^{5/3} T_{\odot}^{2/3}\,\frac{1}{1-e^2}\,\frac{m_c\,(4\,m_p + 3\,m_c)}{2\,(m_p + m_c)^{4/3}},$$

where $T_{\odot} = \frac{G\,M_{\odot}}{c^3} \approx 4.925\ \mu s$.

- m_p, m_c mass of the pulsar and its companion.
- P_b, e orbital period and eccentricity.

Candidates

Pulsar	P (ms)	$\dot{E}$ (10^{26} W)	Ω_p (deg/yr)	χ	i	δ	References
J0737-3039A	22.7	5.9	4.8	90	90	$\lesssim 6$	(Ferdman et al., 2013)
J0737-3039B	2773	0.0017	5.1	70	90	138	(Perera et al., 2010)
J1906+0746	144	270	2.2	81	42-51	89	(Desvignes et al., 2013)
B1913+16	59	1.7	1.2	47	157	21	(Weisberg & Taylor, 2002)
B1534+12	37.9	1.8	0.5	110	78	30,100?	(Konacki et al., 2003)
J1141-6545	394	2.8	1.4	160	73	93	(Manchester et al., 2010)

Table: Approximate orbital parameters for some double neutron stars. Angles are given in degrees according to the fits given in the corresponding references.

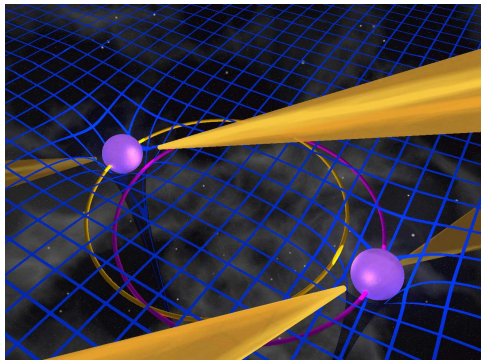

The double pulsar.

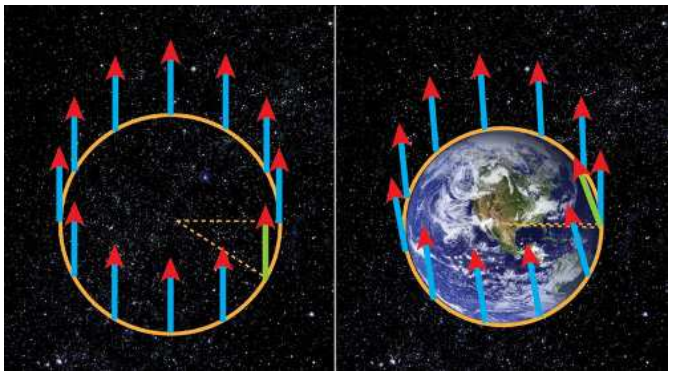

Illustration of geodetic precession.

Striped wind

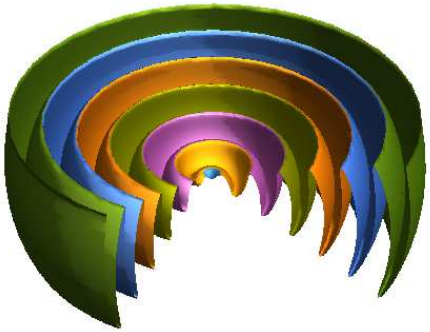

Magnetic field structure with current sheet of thickness L in spherical coordinates

$$B_r = \beta_{\rm v}^2 B_{\rm L} \frac{r_{\rm L}^2}{r^2} \tanh(\Psi_s/L)$$

$$B_\vartheta = 0$$

$$B_\varphi = -\beta_{\rm v} B_{\rm L} \frac{r_{\rm L}}{r} \sin\vartheta \tanh(\Psi_s/L)$$

Figure: Striped wind geometry.

Location of the current sheet in space and time:

- solid body rotation at the stellar speed Ω.
- relativistic radial motion with speed $\beta_{\rm v}\, c$.

$$\Psi_s = \cos\vartheta \cos\chi + \sin\vartheta \sin\chi \cos\left[\varphi - \Omega\,(t - \frac{r}{\beta_{\rm v}\, c})\right]$$

represents an exact solutions to the homogeneous Maxwell equations.

(Pétri, 2011; Petri, 2012; Pétri, 2013, 2015)

Phase plots of the striped wind

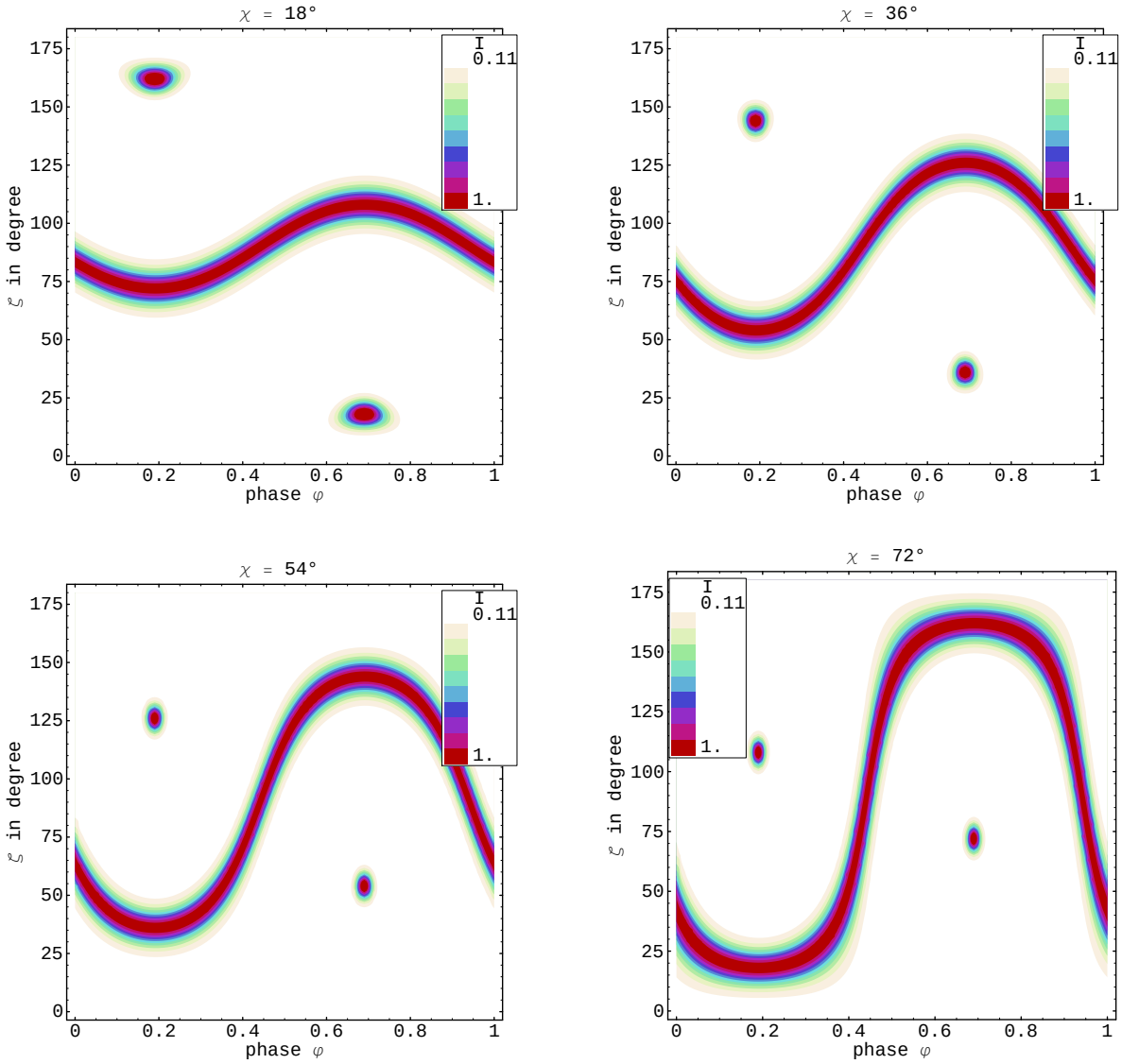

Figure: Phase plot of the pulsed gamma-ray and radio emission components (Pétri, 2011).

Evolution of pulse profile

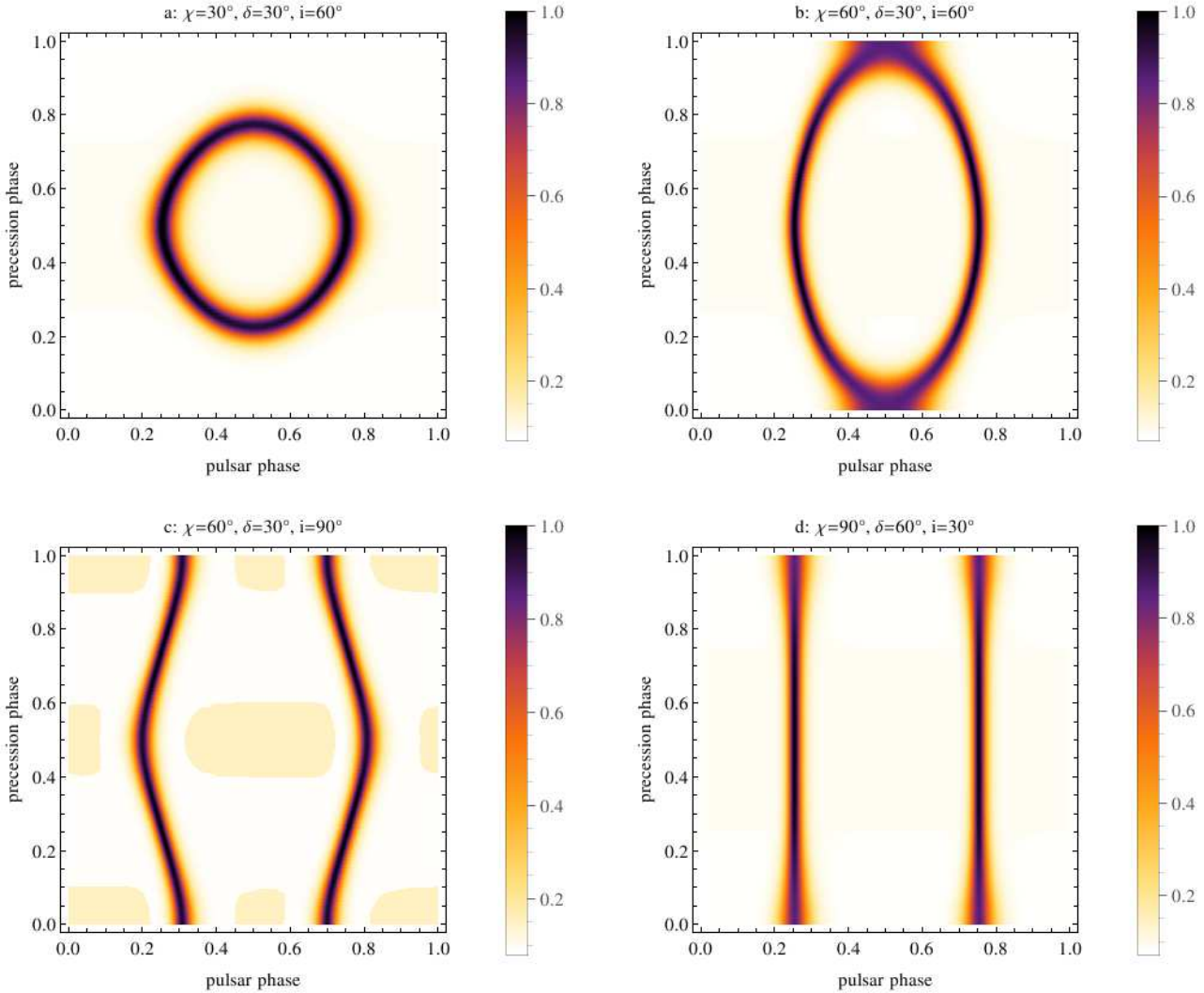

Figure: Evolution of the pulse profile with respect to the precession phase φ for several geometries of the binary pulsar.

Evolution of peak separation

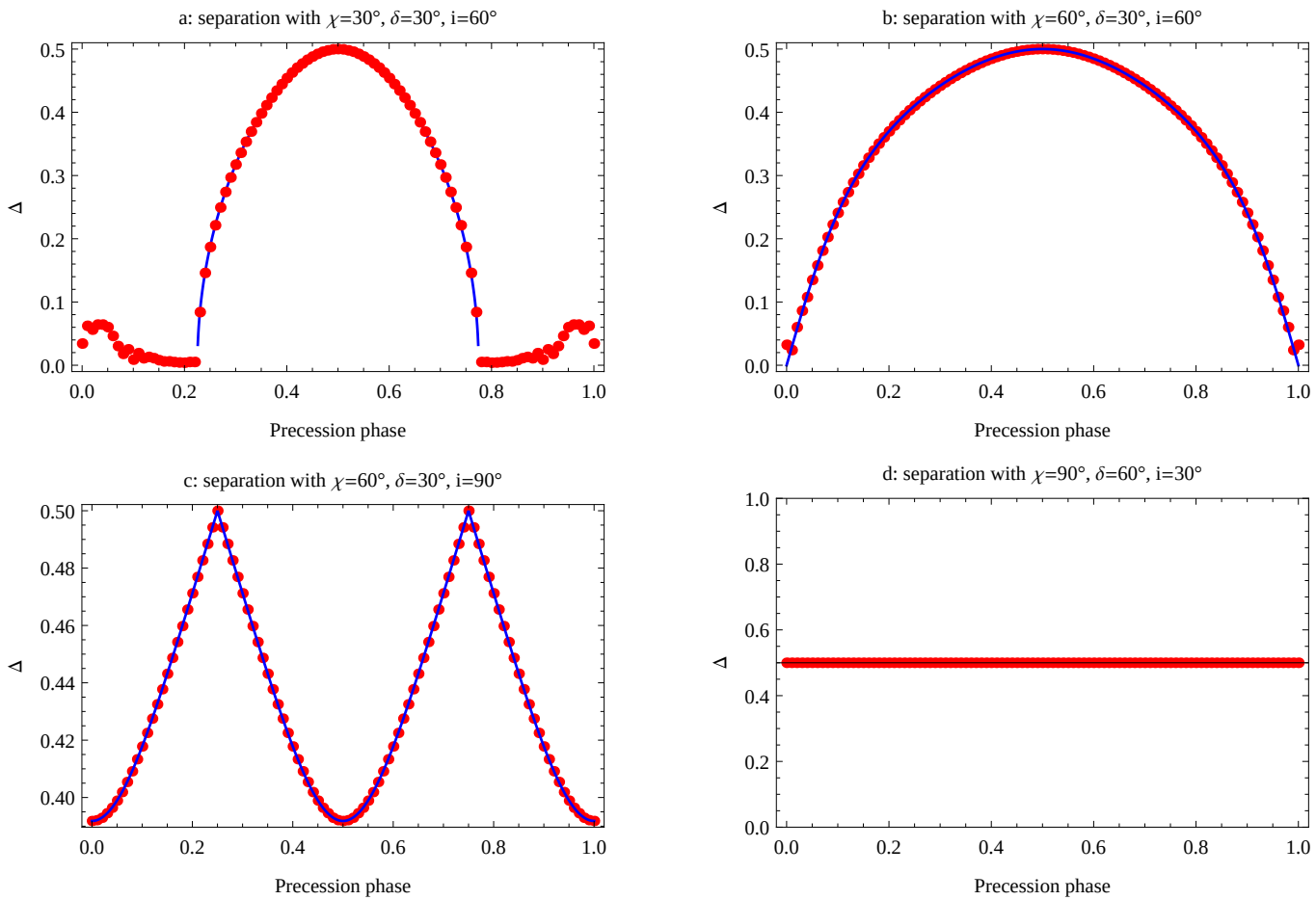

Figure: Simulated evolution of the peak separation Δ with respect to the precession phase φ compared with predictions.

Evolution of pulse width

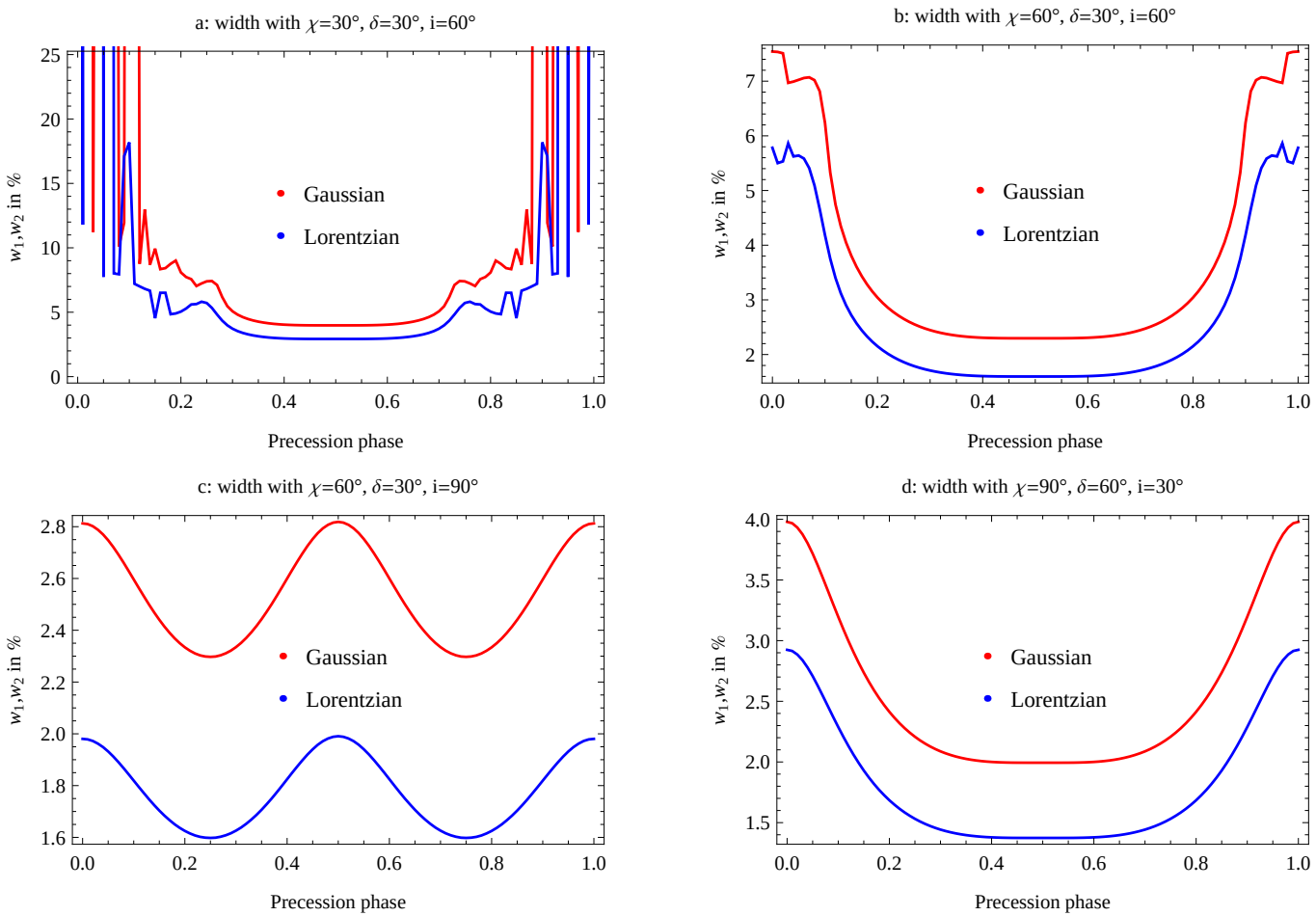

Figure: Evolution of the pulse width (w_1, w_2) with respect to the precession phase φ. The two fitting models are shown, Gaussian in red and Lorentzian in blue.

Evolution of peak amplitude

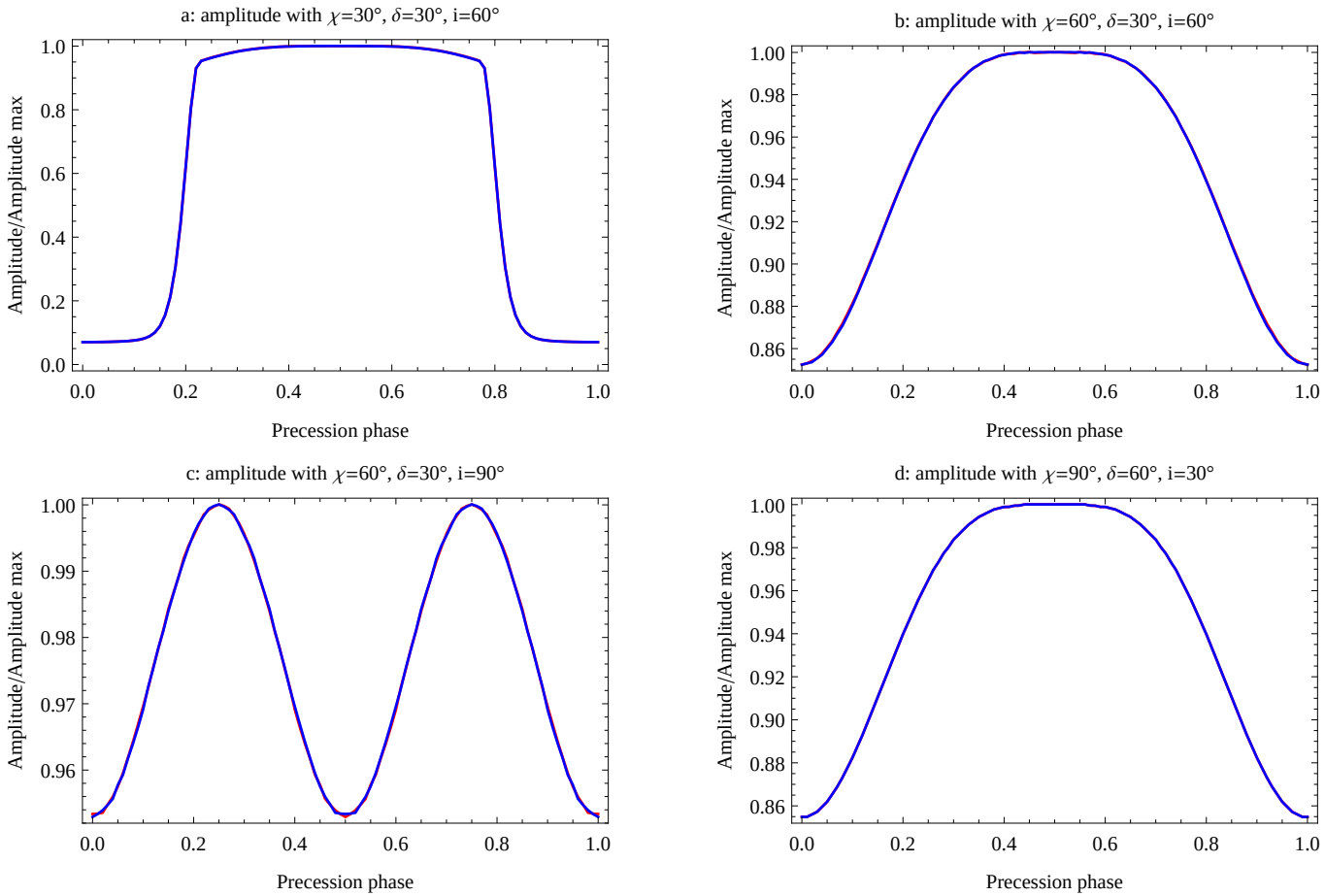

Figure: Simulated evolution of the highest peak amplitude $I_{\max}$ with respect to a full precession period with phase $\varphi \in [0, 2\,\pi]$. The two fitting models are shown, Gaussian in red and Lorentzian in blue. Both fits overlap almost perfectly.

Comparing competing models of high-energy emission

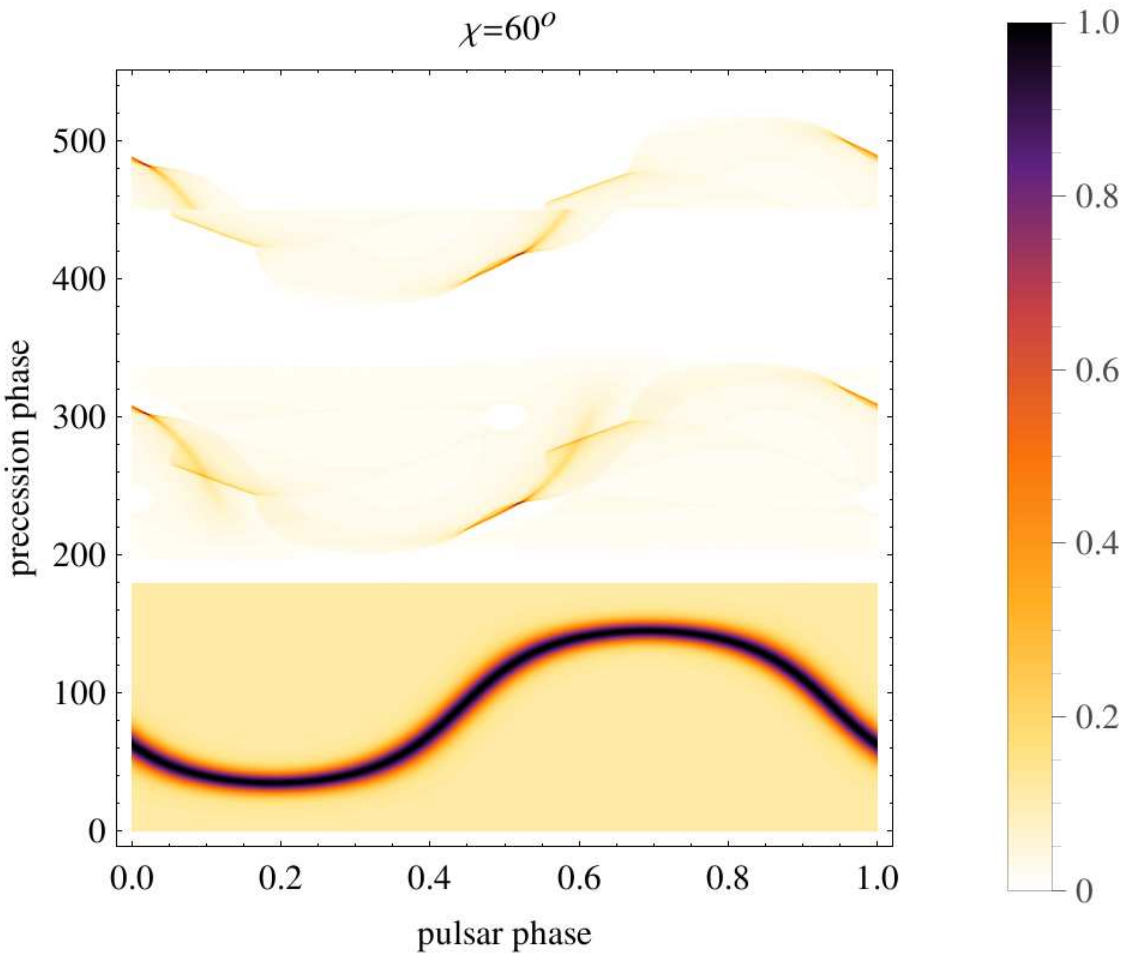

Figure: Phase plot diagram for our striped-wind model, in the lower panel for $\zeta \in [0^o, 180^o]$, the two-pole caustic model in the middle panel for $\zeta \in [180^o, 360^o]$, and the outer-gap model in the upper panel for $\zeta \in [360^o, 540^o]$. The plots have been artificially shifted to place them in one graph. The pulsar obliquity is $\chi = 60^o$.

The case of PSR J1141-6545

We study in detail PSR J1141-6545 as observed by (Hotan et al., 2005; Manchester et al., 2010; Antoniadis et al., 2011).

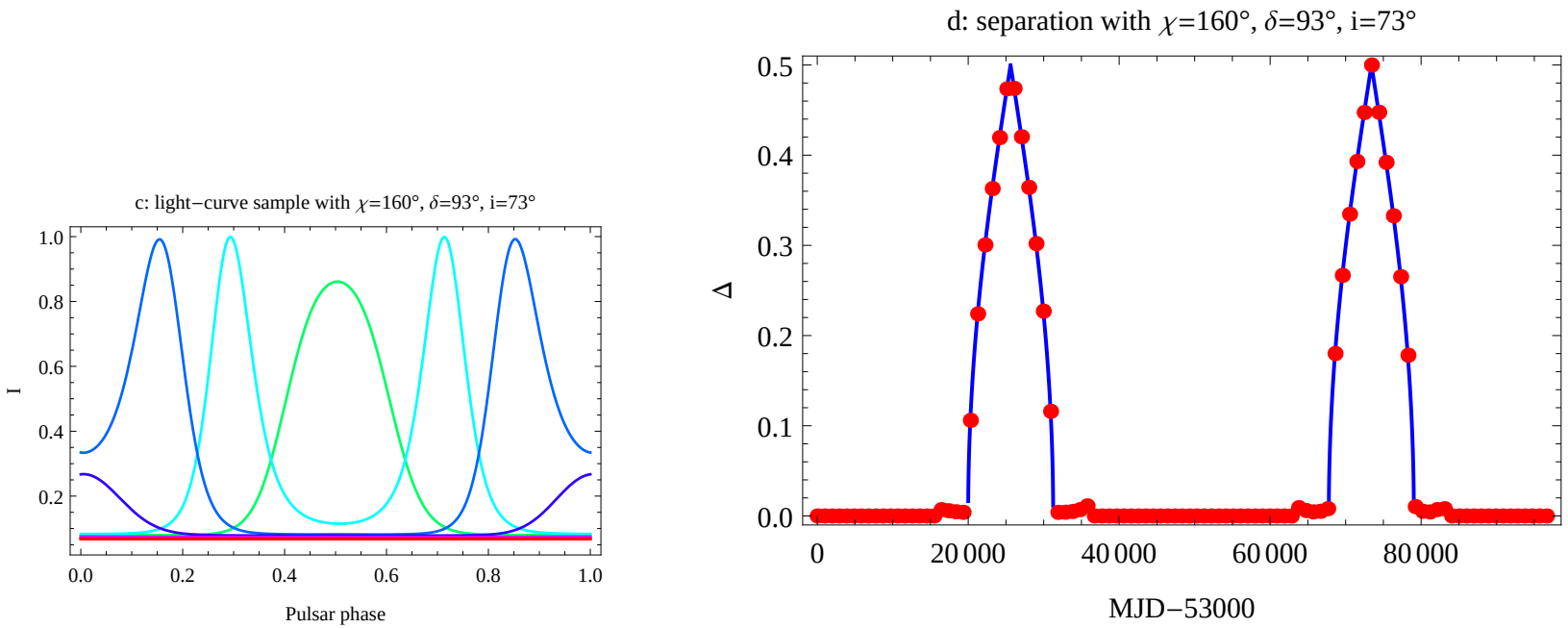

Figure: Analysis of the evolution of the pulsed emission from PSR J1141-6545. Note the different x-label, pulsar phase for the width of the pulses (left) but precession phase for the separation of the two peaks (right).

Pulse profile evolution for PSR J1141-6545

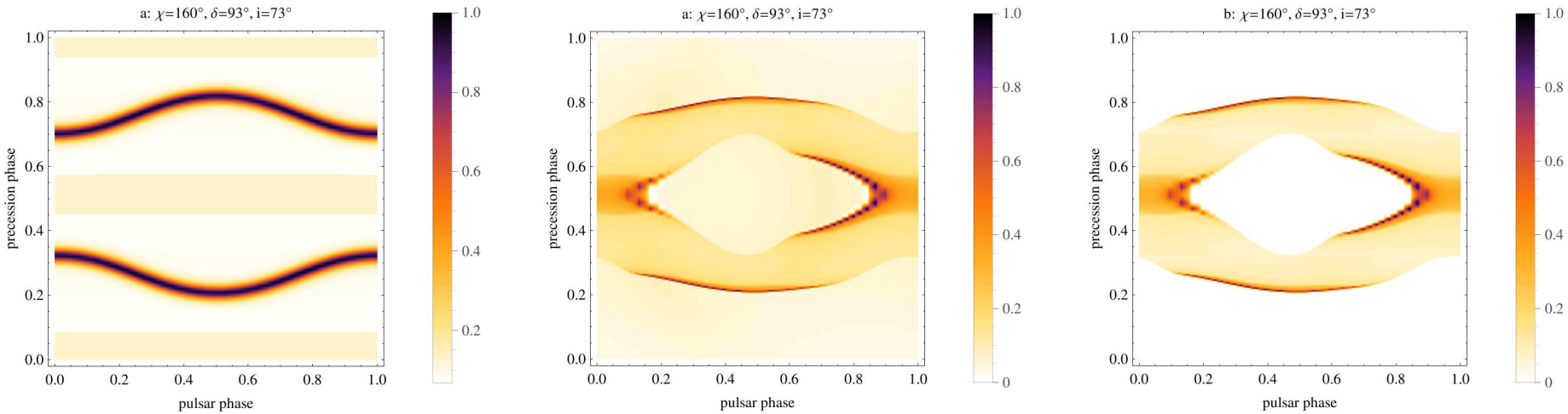

Figure: Evolution of the pulse profile with geodetic precession phase φ for the 3 competing models: striped wind (SW) on the left, two-pole caustics (TPC) in the middle and outer gap (OG) on the right.

Peak intensity variation for PSR J1141-6545

Evolution of the peak intensity with the geodetic precession phase φ for PSR J1141-6545.

Notable differences within one precession period

- SW shows two emission phases around 0.3 and 0.7.
- OG and TPC show three emission phases around 0.2, 0.5 and 0.8.

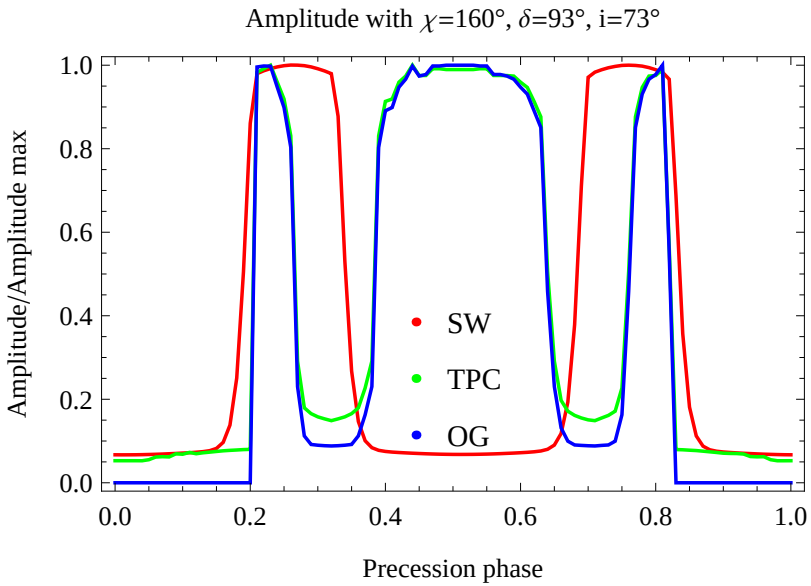

Figure: Predictions for the SW, TPC and OG.

Drastic peak intensity variation alone can already discriminate between the models.

No need for detection of peak phase shift with precession phase!

Peak intensity variation for other candidates

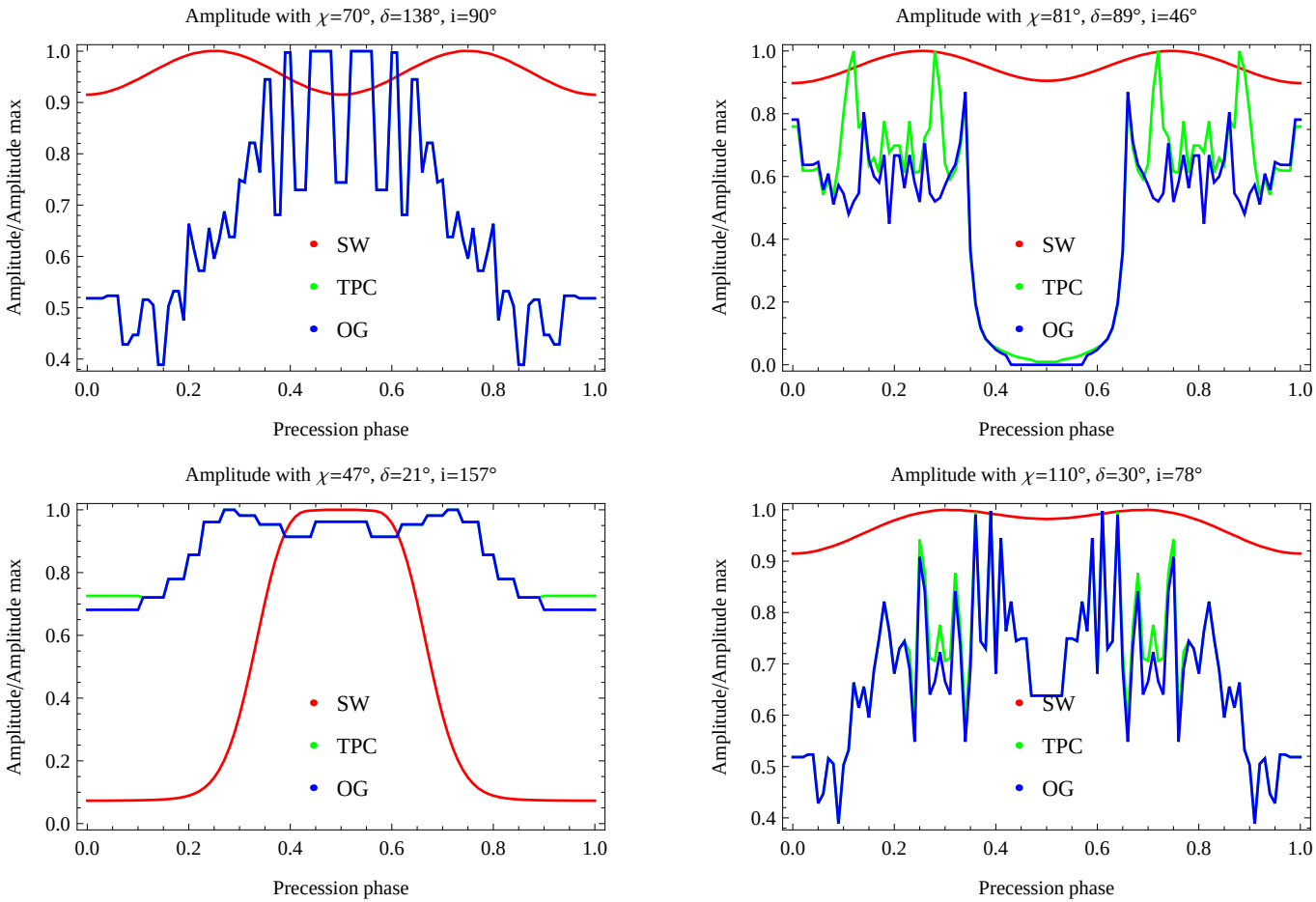

Figure: Evolution of the pulse profile with geodetic precession phase φ for the 3 competing models: striped wind (SW) on the left, two-pole caustics (TPC) in the middle and outer gap (OG) on the right.

Conclusions & Perspectives

- significant change in pulse profile as a result of geodetic precession is expected in X-rays and gamma-rays.
- main differences between competing high-energy models are highlighted.
- geodetic precession imprints a clear signature on high-energy pulse profile evolution.
  $\Rightarrow$ such detections will help constrain the high-energy pulsed emission models for pulsars.
- some predictions about possible future detection of high-energy emission from double neutron star systems are made.
- such observations will definitely favour some pulsed high-energy emission scenarios.
- PSR J1906+0746 and PSR J1141-6545: best candidates to look for geodetic precession in gamma-ray energies and accessible with current telescopes.
- our predictions indicate that within a few decades this emission will be detected with existing technology.

Bibliography

Antoniadis J., Bassa C. G., Wex N., Kramer M., Napiwotzki R., 2011, MNRAS, 412, 580

Damour T., Taylor J. H., 1992, Physical Review D, 45, 1840

Desvignes G., Kramer M., Cognard I., Kasian L., van Leeuwen J., Stairs I., Theureau G., 2013, 291, 199

Ferdman R. D. et al., 2013, ApJ, 767, 85

Hotan A. W., Bailes M., Ord S. M., 2005, ApJ, 624, 906

Konacki M., Wolszczan A., Stairs I. H., 2003, ApJ, 589, 495

Kramer M., 1998, ApJ, 509, 856

Manchester R. N. et al., 2010, ApJ, 710, 1694

Perera B. B. P. et al., 2010, ApJ, 721, 1193

Pétri J., 2011, MNRAS, 412, 1870

Petri J., 2012, MNRAS, 424, 2023

Pétri J., 2013, MNRAS, 434, 2636

Pétri J., 2015, A&A, 574, A51

Weisberg J. M., Taylor J. H., 2002, ApJ, 576, 942